Characterization of Conditions Required for X-Ray Diffraction Experiments with Protein Microcrystals

Robert Glaeser,*†‡ Marc Facciotti,§ Peter Walian,† Shahab Rouhani,§ James Holton,* Alastair MacDowell,¶ Richard Celestre,¶ Daniela Cambie,¶ and Howard Padmore¶

*Department of Molecular and Cell Biology; †Life Sciences Division and ‡Physical Biosciences Division, Lawrence Berkeley National Laboratory; §Graduate Group in Biophysics; and ¶Experimental Systems Group, Advanced Light Source, Lawrence Berkeley National Laboratory, University of California, Berkeley, California 94720 USA

ABSTRACT The x-ray exposure at which significant radiation damage occurs has been quantified for frozen crystals of bacteriorhodopsin. The maximum exposure to ~11-keV x-rays that can be tolerated for high-resolution diffraction experiments is found to be $\sim 10^{10}$ photons/μm^2, very close to the value predicted from limits that were measured earlier for electron diffraction exposures. Sample heating, which would further reduce the x-ray exposure that could be tolerated, is not expected to be significant unless the x-ray flux density is well above 10^9 photons/s-μm^2. Crystals of bacteriorhodopsin that contain $\sim 10^{11}$ unit cells are found to be large enough to give ~100 high-resolution diffraction patterns, each covering one degree of rotation. These measurements are used to develop simple rules of thumb for the minimum crystal size that can be used to record x-ray diffraction data from protein microcrystals. For work with very small microcrystals to be realized in practice, however, it is desirable that there be a significant reduction in the level of background scattering. Background reduction can readily be achieved by improved microcollimation of the x-ray beam, and additional gains can be realized by the use of helium rather than nitrogen in the cold gas stream that is used to keep the protein crystals frozen.

INTRODUCTION

Synchrotron sources provide a number of well-recognized advantages for protein crystallography experiments. Among the key features one can mention are extremely rapid data collection, routinely higher resolution, the opportunity to tune the x-ray wavelength to an absorption edge for multiple anomalous dispersion (MAD) phasing, and the ability to use much smaller crystals than is practical with a laboratory source.

The ability to conduct diffraction experiments with protein microcrystals can open up a number of important opportunities. Microcrystals can be used to evaluate the quality of diffraction at an early stage, before extensive effort is invested in improving the crystal size. If microcrystals are large enough to allow many diffraction patterns to be collected without severe radiation damage, there is no need to further optimize the conditions to produce larger crystals. These and other reasons for the development of microcrystal diffraction cameras have been discussed recently by Cusack et al. (1998). A possible, further benefit, yet to be tested, could be that very small crystals can be frozen without the use of added cryoprotectants, as is the case for protein crystals used in electron diffraction studies (Taylor and Glaeser, 1974).

Received for publication 20 September 1999 and in final form 13 February 2000.

Address reprint requests to Dr. Robert M. Glaeser, MCB/Biochemistry and Molecular Biology, University of California–Berkeley, Stanley/Donner ASU, Berkeley, CA 94720. Tel.: 510-642-2905; Fax: 510-486-6488; E-mail: rmglaeser@lbl.gov.

0006-3495/00/06/3178/08 $2.00

Experimental work with protein microcrystals—defined here as crystals that are only a few tens of micrometers on edge—can be facilitated by focusing the x-ray beam to ~1/10 the usual size (Bilderback et al., 1994; Pebay-Peyroula et al., 1997). Focusing to a smaller size increases the x-ray flux density at the crystal, an important consideration because the exposure required to produce adequate count statistics in the diffraction spots scales inversely with the crystal volume. Use of a narrow x-ray beam, comparable in size to the protein microcrystal itself, also helps to reduce the background scattering from material surrounding the crystal and from the air in the path between the collimator and the beam stop.

Radiation damage ultimately places a limit on the smallest protein crystal size that can be used for high-resolution data collection, however. A given number of x-rays must pass through a crystal, regardless of its size, to produce a desired number of counts in each diffraction spot. Thus, as the number of unit cells in a crystal decreases, the x-ray exposure per unit cell must increase proportionately. Finally, when the crystal size is too small, radiation damage will destroy the crystal before an adequate exposure has been completed (Henderson, 1990; Gonzales and Nave, 1994).

In anticipation of work that will be done with protein microcrystals at the Advanced Light Source at the Lawrence Berkeley National Laboratory, we have further characterized the limitation on crystal size that is imposed by radiation damage. We find that crystals of bacteriorhodopsin are severely damaged at resolutions better than 3 Å (and significant damage is apparent at lower resolution) after an exposure of $\sim 10^{10}$ photons/μm^2. The damage "threshold" of 10^{10} photons/μm^2 that we measure at ~3-Å resolution is

within a factor of 2 of the value that was estimated by Henderson (1990) from earlier measurements made in electron diffraction experiments. As a conservative rule-of-thumb, we estimate that at least one high-resolution diffraction pattern, covering 1° of rotation, can be obtained from a protein crystal if the crystal size (in micrometers) is 1/10 the unit cell size (in Angstroms). Data covering more than 100° of rotation can therefore be obtained if the crystal size (in micrometers) is 1/2 the unit cell size (in Angstroms). The need to minimize the air-scatter background becomes apparent as the crystal size is reduced to very small dimensions, however.

MATERIALS AND METHODS

Measurements of radiation damage on bacteriorhodopsin crystals were carried out with equipment set up on beamline 7.3.3 of the Advanced Light Source (ALS) at the Lawrence Berkeley National Laboratory (LBNL). The experiment is illustrated schematically in the beamline layout shown in Fig. 1. The toroidal mirror, located 16 m from the source, collected bending magnet radiation and focused it to a spot in the sample at the 37-m location. This mirror provides the full amount of horizontal focusing, resulting in a convergence angle of 2.3 mrads. This mirror provides only a small amount of vertical focusing, however. Most of the vertical focusing is provided by the microfocus mirror located 12 cm in front of the sample. This mirror was of a design similar to those used elsewhere at the ALS (MacDowell et al., 1997). Briefly, it consists of a flat, platinum-coated, fused silica substrate that is bent asymmetrically by means of end couples that are applied by strip springs. The resulting vertical convergence angle onto the sample was 2.5 mrads. A double crystal Ge (111) monochromator, located 1 m in front of the sample, was set to produce 11-keV photons with an energy bandpass of ~1:1000.

It should be noted that this temporary configuration was a test setup and is far from optimum. The flux density on the sample is reduced from the ideal value for two reasons. 1) The conjugates of the toroidal mirror were not set at 1:1 because of positional constraints. This results in an increase in the beam focus size and about an eightfold decrease in flux density at the sample. 2) The Ge (111) monochromator was poorly cooled and suffered from thermal strain that reduced throughput by about fivefold. Despite this, the focused spot size at the sample was measured to be 300 × 54 μm (FWHM). To further reduce the horizontal spot size in a controlled manner, motorized slits (Newport Corp.) were positioned 6 cm in front of the sample, followed by a 300-μm lead pinhole to act as a scatter guard.

A spot size of 130 × 54 μm (FWHM) with a total flux of 2.2×10^9 photons/s (400-mA ring current) was used for the measurements of radiation damage. An even smaller spot size of 48 × 54 μm was used to reduce the background scattering for diffraction from very small crystals. The x-ray spot size was measured by allowing the x-rays to illuminate a YAG phosphor. The visible light image of the beam was projected with magnification onto a CCD camera. The flux measurements were determined using a silicon photodiode (International Radiation Detectors). This device was calibrated against a scintillator detector (Bicron Corp) when operated with low-input flux (<50 kHz). The scintillator detector was considered to be 100% efficient with 11-keV photons at such low count rates. The cross-calibrated photodiode output current was extrapolated to higher currents for the high-flux measurements noted earlier.

A Newport single axis goniometer was mounted on a motorized stage that was equipped with *x* and *y* drives to make the spindle axis coincident with the x-ray beam. Additional motor drives were provided on the goniometer head itself, making it possible to remotely position the protein crystals on the goniometer axis. An Infinity K2 long working-distance microscope (Infinity Phot-Optical Co.) was used to view the sample during alignment. A MSC sample cooler was operated at a specimen temperature of ~170 K. An ADSC Quantum 4 CCD camera (Area Detector Systems Corp.), borrowed from the ALS Macromolecular Crystallography Facility, was used to record the diffraction patterns. Diffraction patterns were indexed, and integrated intensities were produced with the HKL-DENZO software suite (Otwinowski and Minor, 1997).

To demonstrate the principle for further reducing the air-scatter background, nitrogen gas was temporarily replaced by helium gas in the cold-gas stream of a protein-crystal sample cooler (Molecular Structure Corporation) on an *R*-axis IV diffractometer. To make this replacement, the external gas input line, which is normally used to flush the cooling coils with N_2 gas during liquid nitrogen fills, was connected to a helium gas tank. The pressure regulator on the helium tank was adjusted to a value of 10–15 psi. At the same time the pump that is used to generate a steady flow of N_2 gas from the liquid nitrogen reservoir was shut off, and the mode selector switch on the cold gas-stream controller was set to "fill," thus allowing the externally supplied helium gas to flow through the liquid nitrogen cooling coils. The gas flow controller gauges for the cold gas and for the outer (sheath) gas streams were set to values of 30 and 15,

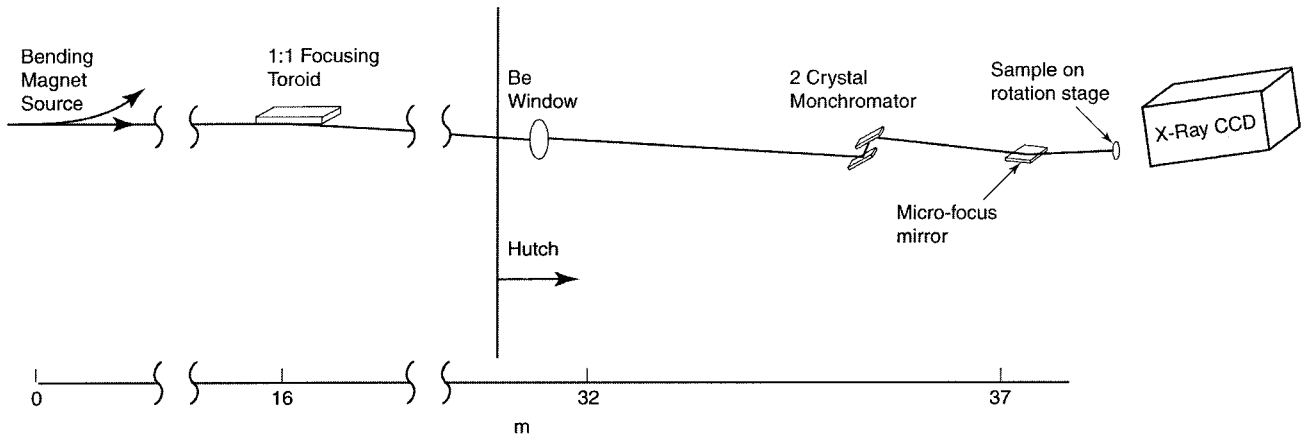

FIGURE 1 Schematic diagram of the diffraction camera assembled for this work. The toroidal mirror collects radiation for beamline 7.3.3 and focuses it to a spot at the sample. Additional vertical focusing was provided by the microfocus mirror located 12 cm in front of the sample. An adjustable slit mounted 6 cm in front of the sample was used to vary the horizontal width of the spot. The double crystal Ge (111) monochromator was used to select ~11-keV photons with a bandpass of 1:1000. Additional details of the sample goniometer, sample cooler, and area detector are described in the text.

respectively. We estimate that two-thirds or more of the path length between the tip of the collimator and the beam stop is effectively "purged" by helium gas in this way.

Crystals of the F219L mutant of bacteriorhodopsin, grown by the lipidic cubic phase technique of Landau and Rosenbusch (1996), were used for our measurements of radiation damage. These crystals were already available because of a program of experimental data collection that is currently under way. Wild-type bacteriorhodopsin crystals grow from the monoolein cubic phase as thin hexagonal plates ($p6_3$; $a = b = 60.8$ Å, $c = 108$ Å), which in most cases are ~10–20 μm thick. While crystals will grow as large as 100 μm × 100 μm or more in area, our setups also contain an abundance of additional crystals in all sizes smaller than that.

RESULTS

The strategy for our measurement of radiation damage was to collect a 10° wedge of data as a series of 10 diffraction patterns, rotating the crystal by 1° for each image recorded on the CCD camera. At the end of such a series, the crystal was returned to its original orientation, and the same 10° wedge was recollected. This process was continued until considerable deterioration of the diffraction pattern became apparent at high resolution. The incident x-ray beam was oriented at ~45° to the crystal face. The small crystal thickness ensures that the decrease in intensity from the front to the back of the crystal, due to absorption, was negligible. Thus the radiation dose (energy deposited per unit volume) was nearly homogeneous throughout the volume of the crystal. The size of the x-ray beam was made slightly larger than the size of the protein crystal to ensure that none of the crystal would rotate outside of the beam for part of the exposure, thus sparing it from damage.

Fig. 2 shows a comparison of the diffraction pattern recorded in frame 10 and the corresponding pattern recorded in frame 70. The pattern obtained in frame 10 is shown in Fig. 2 *A* (central, low-resolution region) and in Fig. 2 *C* (example of the high-resolution region). Identical regions of the diffraction pattern recorded in frame 70 are shown in Fig. 2, *B* and *D*, respectively. It is clear that most of the high-resolution diffraction spots that were originally present in the first 10° wedge of data have been lost by the time that the seventh wedge was recorded. The fading of diffraction spots due to radiation damage is represented in more quantitative terms by the intensity statistics shown in Table 1. The number of reflections with measured intensities less than a given factor times σ, the error estimated by the program SCALEPACK (Otwinowski and Minor, 1997), is shown in this table for different resolution shells. Table 1

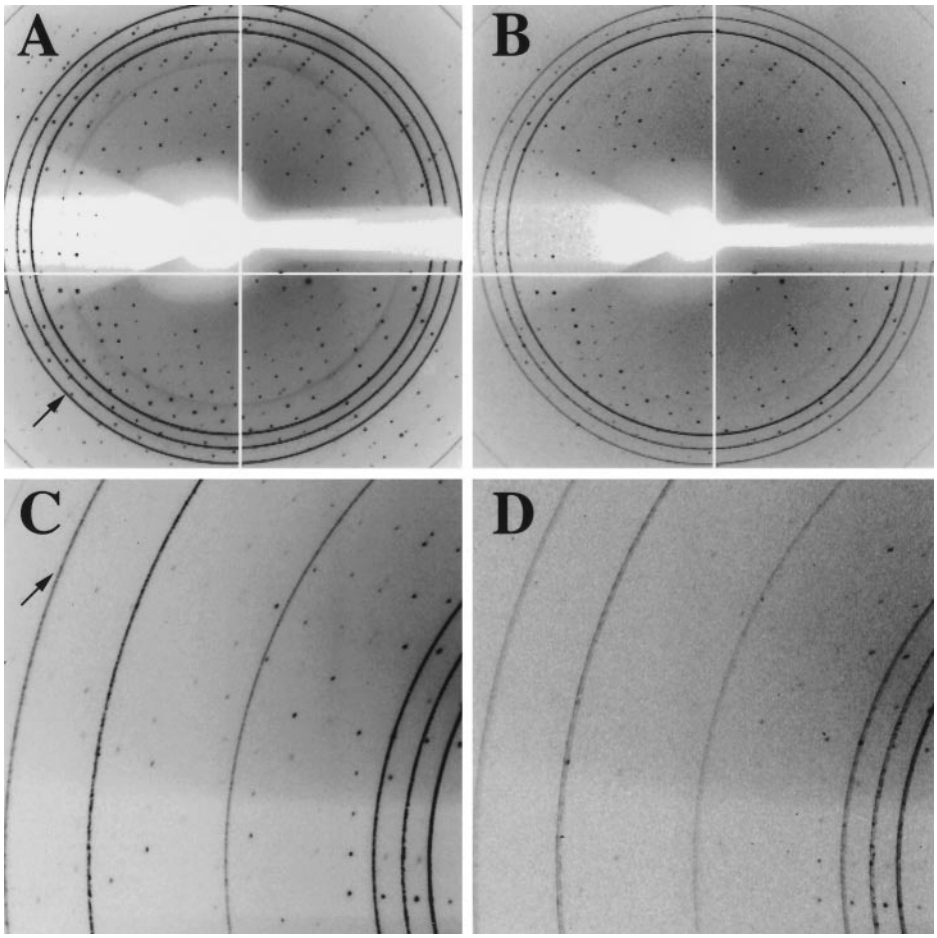

FIGURE 2 Comparison of equivalent diffraction patterns recorded from the same bacteriorhodopsin crystal early in the radiation damage series (*A* and *C*) and at the end of the radiation damage series (*B* and *D*). All panels in this figure show images of 1° rotation photographs recorded with the same crystal orientation. The high-resolution segments of the diffraction patterns (*C* and *D*, respectively) are shown with increased magnification to optimize the visual presentation of diffraction spots. The sharp ring marked by an arrow in *A* lies at a Bragg spacing of 3.4 Å, while the ring marked by an arrow in *C* lies at a Bragg spacing of 2.0 Å. This figure is shown to give a qualitative impression of the extent of damage that has developed after an exposure of $\sim 10^{10}$ photons/μm^2. Quantitative comparisons of the complete set of data are given in Table 1 and in Fig. 3.

TABLE 1 Intensity statistics

Shell lower limit (Å)	Shell upper limit (Å)	No. of reflections with I/σ less than								
		0	1	2	3	5	10	20	>20	Total
A. I/σ in resolution shells after 1.62×10^9 hν/μm^2										
15	5.6	9	13	17	18	21	57	283	0	283
5.6	4.49	0	0	0	0	3	26	329	2	331
4.49	3.93	0	0	0	3	4	28	321	3	324
3.93	3.58	1	2	3	4	7	15	77	0	77
3.58	3.32	0	0	0	0	3	32	133	0	133
3.32	3.13	1	4	6	12	26	109	323	0	323
3.13	2.97	2	2	3	9	29	152	336	0	336
2.97	2.85	3	4	8	17	30	195	313	0	313
2.85	2.74	1	6	21	32	52	224	326	0	326
2.74	2.64	1	6	10	17	38	155	214	0	214
2.64	2.56	4	7	14	30	60	181	216	0	216
2.56	2.49	4	19	31	52	95	278	313	0	313
2.49	2.42	4	14	37	71	124	267	306	0	306
2.42	2.36	10	27	49	65	123	298	325	0	325
2.36	2.31	14	36	59	86	145	290	313	0	313
2.31	2.26	13	27	53	82	162	293	319	0	319
2.26	2.22	2	9	13	23	33	57	60	0	60
2.22	2.17	11	26	48	66	109	176	189	0	189
2.17	2.14	20	46	77	114	182	288	297	0	297
2.14	2.1	17	39	78	121	197	311	325	0	325
All HKL		117	287	527	822	1443	3432	5318	5	5323
B. I/σ in resolution shells after 9.69×10^9 hν/μm^2										
15	5.6	8	16	20	24	43	137	227	0	227
5.6	4.49	2	2	6	11	24	115	251	1	252
4.49	3.93	1	2	6	11	22	106	254	1	255
3.93	3.58	2	6	7	11	22	56	72	0	72
3.58	3.32	2	5	7	21	52	99	113	0	113
3.32	3.13	11	30	58	90	145	246	256	0	256
3.13	2.97	13	34	73	110	173	236	240	0	240
2.97	2.85	18	50	82	115	175	226	229	0	229
2.85	2.74	24	63	98	140	193	227	228	0	228
2.74	2.64	26	58	92	122	161	196	197	0	197
2.64	2.56	32	70	105	136	158	180	180	0	180
2.56	2.49	47	83	135	175	213	221	221	0	221
2.49	2.42	31	80	131	180	203	208	208	0	208
2.42	2.36	31	84	124	163	185	188	188	0	188
2.36	2.31	46	91	142	169	190	195	195	0	195
2.31	2.26	40	90	145	173	199	200	200	0	200
2.26	2.22	5	10	15	17	24	24	24	0	24
2.22	2.17	31	58	77	88	99	101	101	0	101
2.17	2.14	48	93	123	146	157	158	158	0	158
2.14	2.1	34	79	121	147	159	159	159	0	159
All HKL		452	1002	1567	2049	2597	3278	3701	2	3703

Intensity statistics provided by the program SCALEPACK in the HKL suite (Otwinowski and Minor, 1997) for identical, 10° wedges of data recorded as (*A*) the first series of 1° rotation photographs and (*B*) the seventh and final series of 1° degree rotation photographs. The total x-ray exposure received by the crystal at the end of each 10° rotation series is stated in the body of the table.

A shows the intensity statistics for the data in the first 10° wedge, and Table 1 *B* shows the intensity statistics for data collected in the seventh cycle.

The same data are again shown in Fig. 3, this time represented as the number of diffraction spots for which I/σ is greater than 5 for three different resolution shells. The number of reflections in each shell is shown as a percentage of the number present in the first 10° wedge of data; the absolute number of reflections found in the first wedge of data is shown in parentheses for each resolution shell. This representation of the data is one in which the overall effects of radiation damage are easily appreciated. The effects of radiation damage are also apparent in a graph of the B-factor as a function of accumulated x-ray exposure (data not shown), but the increase in B-factor is less dramatic than might be supposed because the intensity of the low-resolution diffraction spots also decreases with accumulated exposure, as can be seen subjectively in Fig. 3.

It seems clear that, in most cases, one would not want to collect data after an exposure of more than 10^{10} photons/μm^2. Thus this value of exposure is roughly the limit of what can be used to collect data at 3-Å resolution. A resolution of 3 Å is also about the value obtained in electron diffraction experiments with two-dimensional bacteriorhodopsin crystals. The limiting exposure measured in our experiments with three-dimensional crystals is indeed close to the value of 1.6×10^{10} photons/μm^2, estimated by Henderson (1990) to be the maximum acceptable exposure on the basis of electron diffraction data.

As is explained in the Discussion section below, our measurements of radiation damage imply that it would be possible to record at least a single high-resolution diffraction pattern from bacteriorhodopsin crystals whose volume is as small as $\sim(7\ \mu\text{m})^3$, containing $\sim 10^9$ unit cells. We have not been able to verify this experimentally, in part because the level of background scattering that existed in the prototype diffraction camera had not yet been optimized and partly because of the long exposure times that would still have been required with our prototype setup.

Data that we were able to obtain with a very small crystal, $25\ \mu\text{m} \times 25\ \mu\text{m} \times 10\ \mu\text{m} = (18.4\ \mu\text{m})^3$, as measured with a high-power dissecting microscope, lend credibility to the above estimate, however, and at the same time demonstrate the need for improvements that can be made over the prototype camera. Fig. 4 *A* shows a 1° rotation photograph obtained with this small crystal with the experimental camera on beam-line 7.3.3, recorded with a 600-s exposure. The x-ray exposure used for this diffraction pattern was estimated to be 3.6×10^8 photons/μm^2, and the x-ray beam size was $\sim 50\ \mu\text{m} \times \sim 50\ \mu\text{m}$. It is evident that the air-scattering background is still a major limitation in the current setup. Fig. 4 *B* shows a similar, 1° diffraction photograph recorded from the same bacteriorhodopsin crystal in 80 s on the protein crystallography camera on beamline 5.0.2 at the ALS, using a 100-μm pinhole collimator. The increase in background, attributable to the less favorable ratio of x-ray beam size to crystal size, is quite conspicuous.

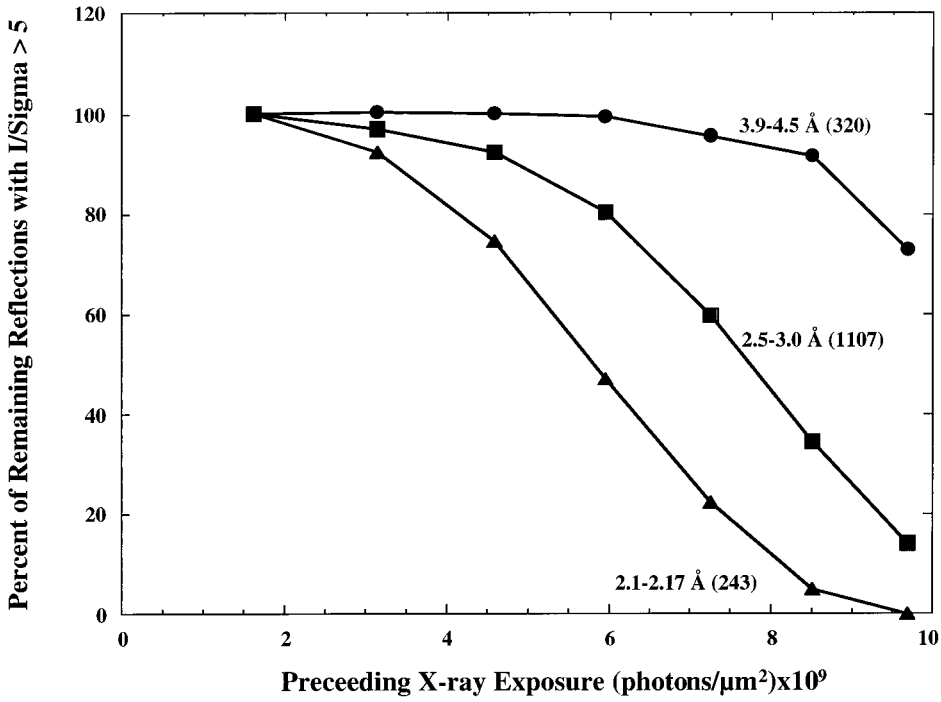

FIGURE 3 Degradation of crystal quality as a function of x-ray exposure. The number of diffraction spots with $I/\sigma > 5$ within a 10° wedge is plotted for three resolution shells, 2.10–2.17 Å, 2.5–3.0 Å, and 3.9–4.5 Å. These numbers are obtained from the SCALEPACK intensity statistics by subtracting the number of reflections with $I/\sigma < 5$ from the total number of reflections in a shell. The total number of diffraction spots with $I/\sigma > 5$ that were found within the first 10° wedge of data is indicated in parentheses for each shell, and the number of diffraction spots found for each shell is presented as a percentage of the number found in the first 10° wedge. From the slope of the curve at low exposure it is apparent that significant damage is already present at 2-Å resolution after an exposure of 2×10^9 photons/μm^2. Damage is severe at a resolution of 3 Å after an exposure of $\sim 10^{10}$ photons/μm^2, and it would appear that the crystal would no longer show diffraction at 4-Å resolution after receiving twice that exposure.

A further reduction of background scattering can be achieved simply by using cold helium gas rather than nitrogen gas, but at the same temperature, to cool the protein crystal. This fact was demonstrated on an *R*-axis IV diffraction camera equipped with the Yale mirrors, for which the x-ray beam size was ~300 μm in diameter. Fig. 5 shows a pair of diffraction patterns obtained with a single bacteriorhodopsin crystal, one photograph taken with nitrogen as the cold gas and the other with helium. The two diffraction patterns were recorded with identical exposure times and with all parameters of the x-ray source held constant. Fig. 5, *A* (nitrogen) and *B* (helium), shows the two diffraction patterns with gray scale and threshold parameters that are optimized separately for each image. This comparison underestimates the benefit of using helium gas in the cold stream, however. Fig. 5, *C* (nitrogen) and *D* (helium), shows how the two images compare when they are displayed with the same gray scale and threshold values, in this case chosen to not favor one image dramatically over the other. Quantitative measurement of the background in the two cases showed about a sixfold reduction achieved with helium at resolutions below 10 Å, a four- to fivefold reduction at resolutions between 7 Å and 10 Å, a three- to fourfold reduction at resolutions between 4 Å and 7 Å, and about a twofold reduction at resolutions between 2 Å and 3 Å. The relatively stronger reduction in the background scattering at low resolution is due, of course, to the fact that the larger diameter of the nitrogen molecule causes the scattering from N_2 to be more strongly concentrated at small angle than is the case for He. If required, even further reduction of the background scattering would be achieved (at all angles) with a more sophisticated, helium-filled enclosure, which would more completely purge the space between the collimator and the beam stop.

DISCUSSION

The maximum x-ray exposure that can safely be given to a frozen bacteriorhodopsin crystal has been measured to be no greater than $\sim 10^{10}$ photons/μm^2, if data are to be collected to a resolution of at least 3 Å. This measurement agrees very closely with the value of 1.6×10^{10} photons/μm^2 predicted by Henderson (1990) on the basis of radiation damage studies that had been done earlier in electron crystallography. It is expected that the radiation dose required to damage a frozen protein crystal will be the same for x-ray exposures as it is for electron exposures, of course, because nearly all of the energy deposited in the sample, in both cases, is the result of inelastic electron-scattering events.

The value of "safe" x-ray exposure that we have measured, however, is ~10 times lower than that estimated by Gonzales and Nave (1994). (We have used the value of 8×10^{17} keV/mm^3 deposited in the sample for a flux of 10^{11} photons/μm^2 to relate the calculated radiation dose given by Gonzalez and Nave to a corresponding x-ray flux.) The difference may be attributed in part to differences in criteria for judging how much exposure can be tolerated. Damage to the protein exhibits no unique threshold, in that it occurs progressively with increasing x-ray exposures, and a given

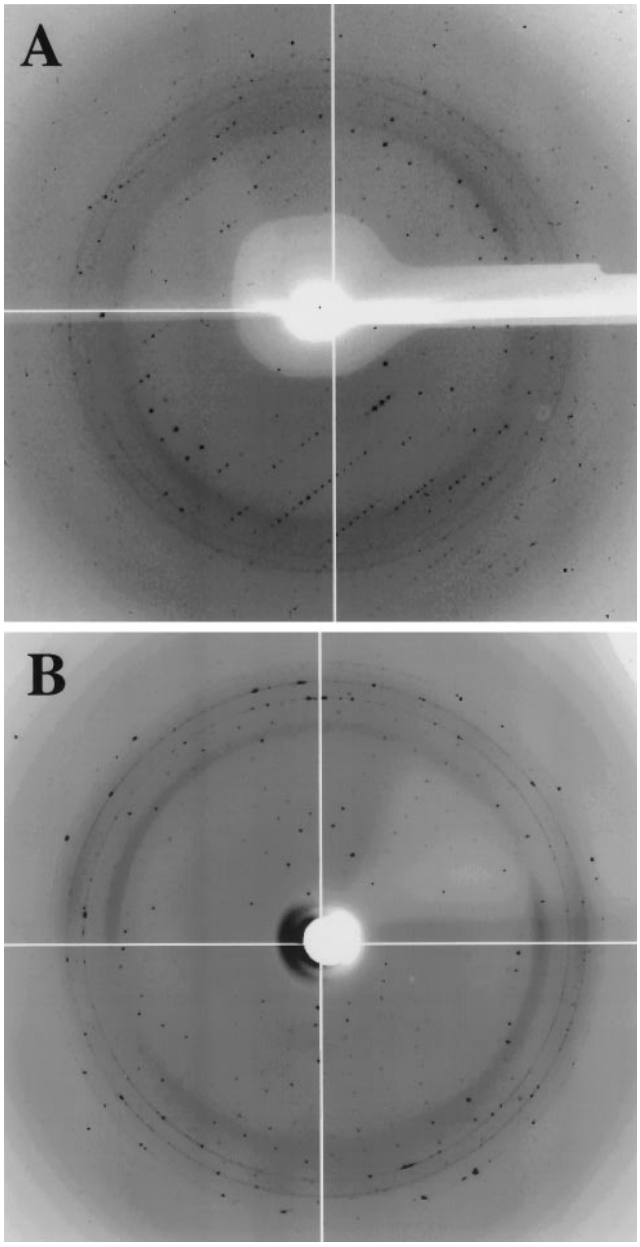

FIGURE 4 One-degree rotation patterns obtained from a bacteriorhodopsin crystal measured to be 25 μm × 25 μm × 10 μm. (*A*) A diffraction pattern obtained from this very small crystal with the experimental microfocus camera on beamline 7.3.3. (*B*) A diffraction pattern obtained from the same crystal on beamline 5.0.2, using a 100-μm collimator. The ice rings visible in *B* are due to frost accumulated on the surface. As the qualitative comparison in this figure shows, the background scattering intensity is already quite high in the pattern obtained with the microfocus camera, and it is markedly worse in the pattern obtained with the 100-μm collimator.

degree of damage occurs much earlier at high resolution than at lower resolution. As noted by Gonzales and Nave, their value of the x-ray exposure that could be tolerated would also tend to be an overestimate because of the way in which they had to calculate the dose delivered by their beam of "white" radiation. The use of monochromatic radiation and very thin protein crystals in our experiments is thus an experimental refinement that was not practical in the earlier measurement made by Gonzales and Nave.

How universal will the limiting, "safe" x-ray exposure prove to be for frozen protein crystals? We can again turn to experience in electron crystallography for an indication of what the answer will be. The maximum exposure that can be used for high-resolution electron diffraction experiments has not been found to differ for various proteins, at least to the accuracy with which it is normally measured. Because damage caused by x-ray exposures is really damage caused by electrons, one can also expect that the maximum tolerated x-ray exposure will not vary from one sample to another. An important caveat, however, is that the x-ray intensity must be kept low enough to prevent an appreciable rise in specimen temperature during the exposure. If x-ray flux densities are high enough to warm the sample, one can expect that damage will occur at even lower exposures than are reported here. Gonzales and Nave report, however, that there was no detectable dose-rate effect for beam intensities high enough to damage the sample after only a few minutes of exposure.

Padmore et al. (manuscript in preparation) have used heat-transfer calculations to further define the conditions under which sample heating can safely be ignored. For any currently practical rate of x-ray exposure, these calculations make it clear that the thermal impedance at the convective boundary between the frozen sample and the cold-gas stream determines how much heating will occur, while the thermal impedance of the sample itself (modeled as being pure ice) makes a negligible contribution to the rise in specimen temperature. For a ~12-keV x-ray flux density of 10^9 photons/s-μm^2, high enough to limit the working time (total allowed exposure time) to ~10 s, one can expect the temperature of a 20-μm-diameter crystal to increase by less than 2 K from the temperature of the cold nitrogen gas, while the temperature of a 200-μm sample would increase by less than ~8 K. The latter value is probably closer to the correct estimate than the former, for small microcrystals if they are mounted within a 100-μm loop, surrounded by mother liquor. The amount of temperature rise can be further reduced by a factor of ~3 relative to the values quoted above if helium gas, cooled to ~100 K, is used in the cold stream. It is clear from these model calculations that specimen heating, which scales as the absorbed power, could become an important consideration if appreciably greater flux densities were used. However, it will rarely be the case that one would want to deliver a fully damaging exposure in times shorter than ~10 s.

Personal experience has frequently been described to us by others that seems not to be consistent with the belief that radiation damage for frozen specimens must be independent of the type of crystal being studied. We urge that two conditions should be met before coming to such a conclusion. 1) Quantitative values of the x-ray flux density should

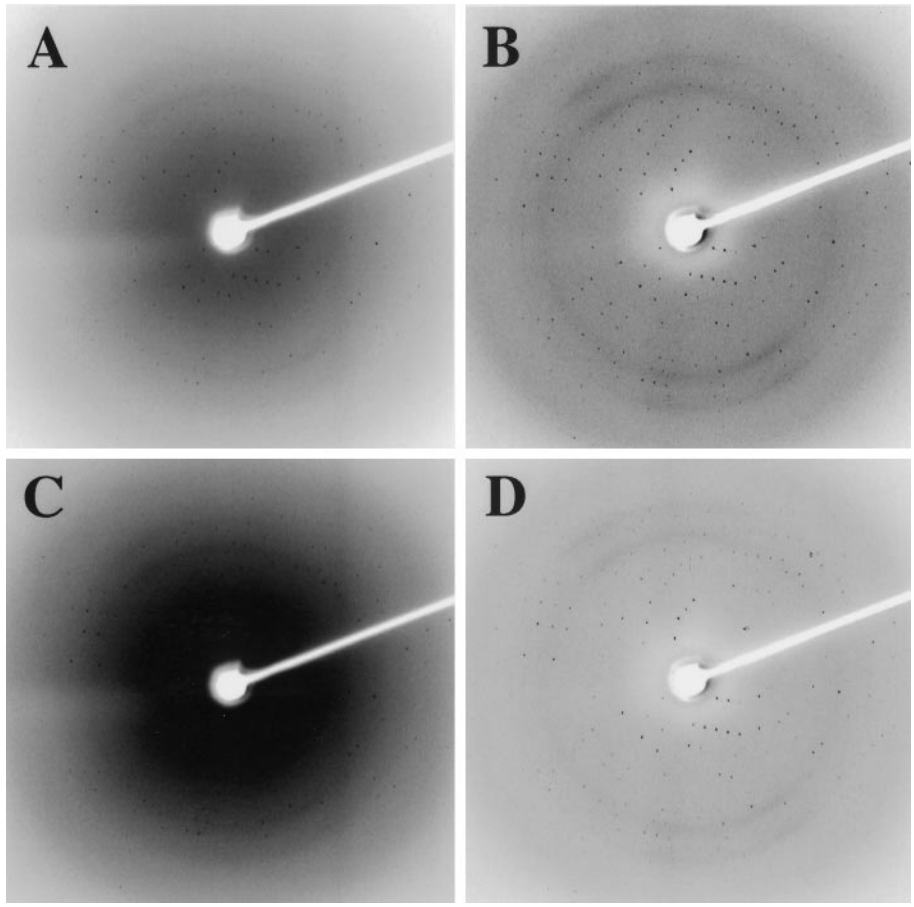

FIGURE 5 Documentation of the reduction in background scattering achieved by using cold helium gas rather than cold nitrogen gas to maintain a frozen protein crystal at a temperature of ~170 K. Diffraction patterns were recorded under otherwise identical conditions of x-ray beam intensity and exposure time, on an *R*-axis IV protein diffraction camera with a focused, 300-μm x-ray spot. The best possible representations of the two diffraction patterns are shown for N_2 (*A*) and for He (*B*). A more accurate representation of the improvement provided by He is given by showing the images with identical gray scale and threshold values, however. This is done in (*C*) for N_2 and in (*D*) for He. Quantitative details regarding the reduction in background scattering that is realized for different resolution shells are given in the text.

be known when the crystal lifetimes observed in one situation are compared to those observed in another situation. 2) The rate at which the protein is destroyed should be measured in units of accumulated x-ray exposure (e.g., photons/μm^2) and not in units of the number of frames of data that could be recorded. The number of frames of data that can be collected, while of practical importance, will vary in the obvious way with unit cell size, which determines the strength of diffraction intensities. In addition, there is a danger—if quantitative values of the flux density are not known—that much longer exposures than necessary are used when the flux density is extremely high, resulting in many fewer frames of data being recorded before severe damage is observed.

Our experience when collecting full data sets from the largest available crystals of bacteriorhodopsin suggests that a crystal must contain at least 10^{11} unit cells to record ~100 high-resolution diffraction patterns at 2-Å resolution, using 1° of rotation for each photograph. The number of high-resolution diffraction patterns that can be recorded for a given x-ray exposure will depend on the signal-to-noise ratio (i.e., I/σ) that one is willing to accept, of course. The measured I/σ, in turn, will depend upon how high the background scattering is, the degree of short-range order in the crystal, and the mosaic spread or other factors that determine the ratio of diffraction spot size to detector pixel size. Nevertheless, we suggest that a value of 10^9 unit cells is a moderately conservative estimate for the smallest crystal that can be used to record just a single diffraction pattern at 2-Å resolution.

Taking the value of 10^9 unit cells as the smallest useful crystal size leads, in turn, to practical rules of thumb that can be used to estimate how big a protein crystal should be to record high-resolution diffraction data. The effective crystal size, L, can be expressed as the cube root of the crystal volume, and the effective unit cell size, a, can be expressed as the cube root of the unit cell volume. If L is then measured in micrometers and a is measured in Angstroms, a crystal of size

$$L = 0.1a \tag{1}$$

will contain 10^9 unit cells, about the minimum size needed to record a high-resolution diffraction pattern for 1° of rotation. While such small crystals would not be of interest for collecting a full data set, one may nevertheless want to use crystals in this size range, if that is all that is available, to screen crystallization conditions before investing further

effort in improving the crystal size. By the same argument, a crystal size

$$L = 0.5a \tag{2}$$

will contain 125 times more unit cells than is needed to record a single diffraction pattern. As a result, a crystal of this size would be large enough to collect a full data set covering 125° of rotation. A further increase in crystal size would be unnecessary, unless proportionately more diffraction patterns must be recorded from a single crystal, as may be the case for multiple anomalous dispersion phasing.

The rule of thumb written in Eq. 2 follows from that written in Eq. 1, if one recognizes that the integrated diffraction intensity scales as the number of unit cells in the crystal. It is obvious that this should be the case, because the scattering cross section of the sample, i.e., the integrated diffraction intensity, must scale as the number of atoms in the sample and thus as the number of unit cells in the crystal. The same conclusion can also be derived from the familiar expression for the integrated intensity, which states that

$$I \propto \frac{V_{\text{crystal}} \cdot F^2}{(V_{\text{unit cell}})^2} \tag{3}$$

where V_{crystal} is the volume of the crystal, $V_{\text{unit cell}}$ is the volume of the unit cell, and F is the structure factor for the unit cell. The average value of F^2 scales in proportion to the number of atoms in the unit cell and therefore as $V_{\text{unit cell}}$. Thus the integrated diffraction intensity scales as the number of unit cells in the crystal, although casual inspection of Eq. 3 might at first be thought to imply otherwise.

Reduction in background scattering is an important, practical consideration when protein crystals become much smaller than about $(40\ \mu\text{m})^3$. We have found a 100-μm pinhole collimator to be satisfactory for bacteriorhodopsin crystals as small as 70 μm × 70 μm × 15 μm, but the background scattering proved to be overwhelming when the crystal size was only 25 μm × 25 μm × 10 μm. For crystals in this size range or smaller it will be possible to use adjustable microfocusing in the vertical direction and adjustable slits in the horizontal direction to reduce the x-ray beam size to ~25 μm in diameter, ~1/4 the area of that used in Fig. 4 *A*. In addition, helium rather than nitrogen can be used in the cold gas stream. The combined effect would provide a large reduction in the background that is derived from air scattering. Some of the background scatter in Fig. 4 *B* comes from the surrounding mother liquor, however, and from the cryo-loop that is used to hold the crystal. Even these contributions could also be reduced by mounting very small crystals on thin fibers or on very thin films of the type used to support much smaller protein microcrystals in electron cryomicroscopy.

We thank the ALS Macromolecular Crystallography Facility for use of the CCD detector, and we are grateful to Dr. Carl Cork and Dr. Gerry McDermott for assistance in the setup and calibration of the detector. We are pleased to thank Tom Alber, James Berger, Thomas Earnest, and Bing Jap for discussing various aspects of this work.

This work was initiated with support from the LBNL Laboratory Director's Research and Development Fund. Additional support was provided by National Institutes of Health grant GM51487 and by the U.S. Department of Energy, Office of Basic Energy Sciences, under contract DOE-AC03-765F00098.

REFERENCES

Bilderback, D. H., S. A. Hoffman, and D. J. Thiel. 1994. Nanometer spatial resolution achieved in hard x-ray imaging and Laue diffraction experiments. *Science.* 163:201–203.

Cusack, S., H. Belrhali, A. Bram, M. Burghammer, A. Perrakis, and C. Riekel. 1998. Small is beautiful: protein micro-crystallography. *Nature Struct. Biol*. (Synchrotron Suppl.)634–637.

Gonzales, A., and C. Nave. 1994. Radiation damage in protein crystals at low temperature. *Acta Crystallogr.* D50:874–877.

Henderson, R. 1990. Cryo-protection of protein crystals against radiation damage in electron and x-ray diffraction. *Proc. R. Soc. Lond. Biol.* 241:6–8.

Landau, E. M., and J. P. Rosenbusch. 1996. Lipidic cubic phases: a novel concept for the crystallization of membrane proteins. *Proc. Natl. Acad. Sci. USA.* 93:14532–14535.

MacDowell, A. A., R. Celestre, C-H. Chang, K. Franck, M. R. Howells, S. Locklin, H. A. Padmore, J. R. Patel, and R. Sandler. 1997. Progress towards sub-micron hard x-ray imaging using elliptically bent mirrors. *SPIE.* 3152:126–135.

Otwinowski, Z., and W. Minor. 1997. Processing of x-ray diffraction data collected in oscillation mode. *Methods Enzymol.* 276:307–326.

Pebay-Peyroula, E., G. Rummel, J. P. Rosenbusch, and E. M. Landau. 1997. X-ray structure of bacteriorhodopsin at 2.5 Angstroms from microcrystals grown in lipidic cubic phases. *Science.* 277:1676–1681.

Taylor, K. A., and R. M. Glaeser. 1974. Electron diffraction of frozen, hydrated protein crystals. *Science.* 186:1036–1037.